OXFORD JOURNAL
OF STUDENT
SCHOLARSHIP

Inertial Loading and Structural Efficiency of Wooden and Aluminum CubeSat Chassis

Vedika Mehra and Nipun Kothare
vedika.mehra09@gmail.com

ABSTRACT

Because chassis mass limits the mass available for payloads and other spacecraft systems, CubeSat structural design must strike a balance between low mass and sufficient safety margin. This study used finite element analysis to compare wooden, full aluminium, and topology-optimised aluminium CubeSat chassis under the same 10 g self-inertial loading condition. The entire aluminium chassis weighed 0.31978 kg and had a 383.6 safety factor. The wooden chassis maintained a factor of safety of 193 with a significantly reduced mass of 0.10802 kg. Topology optimisation maintained a factor of safety of 220 while reducing the aluminium chassis mass by 34% to 0.211 kg.

A 66.2% mass reduction would have been necessary for an equal-mass aluminium design. Nevertheless, structural continuity was lost as a result of optimisation at this level, which affected the current chassis configuration. Thus, the continuous optimised configuration utilised for the final structural analysis was represented by the 34% reduction. Despite being almost twice as heavy, the optimised aluminium chassis only maintained a slight factor-of-safety advantage over wood. Wood offered the superior combination of low structural mass and high factor of safety under the modelled conditions, highlighting the significance of assessing CubeSat chassis materials using safety margin in addition to mass rather than absolute material strength alone.

Keywords: CubeSat, finite element analysis, topology optimization, aluminum chassis, wooden chassis, structural mass, factor of safety

INTRODUCTION

CubeSat Structural and Mass Requirements

Originally created for educational missions, CubeSats are standardised nanosatellites that are currently utilised for deep-space exploration, communications, scientific research, Earth observation, and technology demonstrations. By combining several units, their standardised modular architecture lowers development complexity and enables the creation of spacecraft of various sizes (Tortora, 2020). Larger configurations are created by combining multiple units in compliance with standardised dimensional and

deployer-interface requirements (Cal Poly, 2022). A 1U CubeSat has a roughly cubic form with dimensions close to 10 cm × 10 cm × 10 cm.

The CubeSat chassis protects the internal components and provides the primary load path through which launch and deployment forces are transferred. During launch, the structure may be exposed to quasi-static acceleration, random vibration, buckling loads, and other dynamic disturbances (Alhammadi et al., 2019). Finite-element analysis is therefore commonly used prior to physical testing or launch; natural frequencies, deformation, stress, buckling resistance, and structural margins are assessed (Elshaal et al., 2024; Park et al., 2021). Accuracy of these predictions is also affected by modelling decisions such as geometric simplification, connection representation, mesh selection and distribution of component masses (Alhammadi et al., 2020).

CubeSat structures must be both strong and stiff but also light, because structural mass takes away from the mass available for payloads, batteries, communications and other onboard components. Lightweight structural concepts can also enhance the usable internal volume and improve the integration of spacecraft subsystems (Capovilla et al., 2020). CubeSat chassis design therefore requires a compromise between structural safety, mass, stiffness, internal volume, manufacturing feasibility and compatibility with the launch deployer.



Figure 1. Representative CubeSat satellites illustrating the standardised modular architecture commonly used for scientific, educational, and technology demonstration missions in Low Earth Orbit (NASA, 2026).

Material Selection in CubeSat Structures

Aluminium alloys, especially 6061 and 7075, are also preferred for CubeSat primary structures due to their desirable balance of strength, stiffness, low manufacturing complexity, and demonstrated aerospace

performance (Elshaal et al., 2024; Lima et al., 2022). The alloys can be machined into precise frame geometries and are compatible with standard rails and deployer interfaces used for CubeSat missions.

The choice of structural materials directly influences the CubeSat's mass, stiffness, natural frequency, stress distribution, and usable payload. Aluminium is a good structural material, but if the chassis geometry is not optimised, the density of this material can result in a large structural mass. The more structure mass, the less mass is left for payloads, batteries, communications, equipment and other subsystems. Other structural concepts and materials have, therefore, been investigated to improve mass efficiency and increase the internal volume available for mission hardware (Capovilla et al., 2020).

Material choice cannot be based on strength considerations alone. A CubeSat chassis has to be stiff and strong enough to withstand the loadings experienced during launch while satisfying requirements in terms of mass, manufacturability, thermal, dimensional and deployer interface. So it is not just the absolute strength that is important, but also the structural performance of the material at the minimum mass that is practical.

Wood as a Lightweight Structural Alternative

The growing number of satellites sent into low-Earth orbit has raised concerns about the atmospheric impacts of spacecraft re-entry. Aluminium parts used for re-entry can oxidise and create aluminium oxide particles that may remain in the upper atmosphere for long periods. Aluminium and other spacecraft-derived metals have already been measured in stratospheric aerosol particles (Murphy et al., 2023). Modelling studies have also indicated that increased satellite re-entry rates could lead to higher concentrations of aluminium oxide in the atmosphere and may affect stratospheric chemistry and ozone levels (Ferreira et al., 2024).

As a result, wood has been studied as a lightweight and possibly more sustainable material for some spacecraft structures. In order to assess hardwood specimens' dimensional stability, surface condition, and resistance to cracking, recent experiments exposed them directly to the space environment outside the International Space Station. Further research into wood for small-satellite structures is supported by the tested hardwoods' adequate integrity during exposure (Murata et al., 2024).

Additionally, when the same chassis geometry is used, wood's significantly lower density compared to traditional aluminium alloys can reduce structural mass. However, wood's structural performance is highly dependent on species, grain orientation, environmental conditioning, and manufacturing quality because it is anisotropic, moisture-sensitive, and more variable than aluminium (Ross, 2010; Forest Products Laboratory, 2021).

Need for a Mass-Constrained Comparison

Because the aluminium chassis is significantly heavier than wood, a direct comparison of the two materials using the same CubeSat geometry does not accurately reflect structural mass efficiency. This

mass difference also influences the inertial load created inside each structure under acceleration-driven loading.

Therefore, lowering the mass of the aluminium chassis while maintaining its primary load paths and structural performance is necessary for a more meaningful comparison. Topology optimisation was employed in this study to eliminate material from less structurally significant regions and reduce the aluminium mass in the direction of the wooden chassis. In aerospace applications, density-based topology optimisation is frequently used to minimise structural mass while maintaining stiffness or compliance (Zhu et al., 2016; Peng et al., 2025; Gao et al., 2024).

Because it assesses whether aluminium maintains a significant factor-of-safety advantage after material removal, the optimised aluminium chassis offers a more pertinent comparison with wood than the full same-geometry aluminium baseline.

Research Objectives

Under the same 10 g self-inertial loading condition, the structural performance and mass efficiency of wooden, full aluminium, and topology-optimised aluminium CubeSat chassis are to be compared. Chassis mass, maximum equivalent von Mises stress, total deformation, and factor of safety are the main points of comparison. Additionally, the study assesses whether topology optimisation can maintain structural continuity and a high factor of safety while reducing aluminium's mass disadvantage. The goal of the analysis is to ascertain whether optimised aluminium maintains a significant structural advantage after material removal and whether a wooden chassis can offer a competitive factor of safety at significantly lower structural mass.

METHODS AND BASELINE STRUCTURAL ANALYSIS

Chassis Geometry

For the baseline wood and aluminium simulations, a standard CubeSat chassis geometry was utilised. The main external frame, side-panel sections, openings, vertical rails, horizontal structural members, and the base interface—which served as a representation of attachment to the deployer—were all included in the model. These characteristics were kept because they control the transfer of launch loads throughout the model and constitute the main load-carrying structure of the chassis.

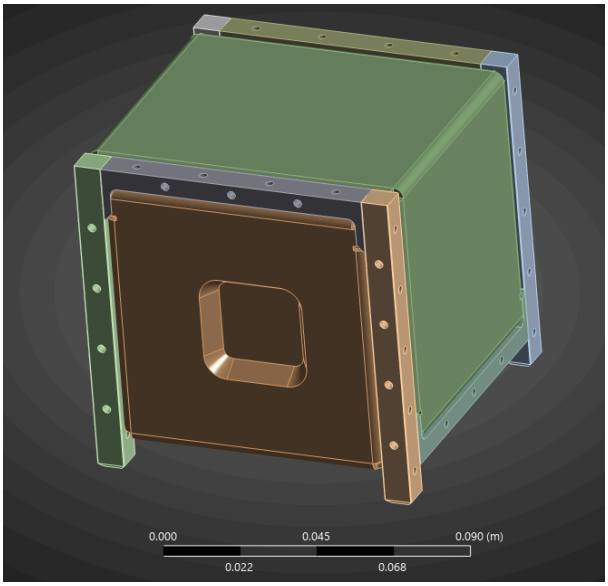


Figure 2. CAD model of the 1U CubeSat chassis used for the baseline finite element analyses of the wooden and aluminium cases.

To ensure that the baseline comparison only showed the impact of material properties, the same CAD geometry was applied to both materials. To enhance mesh generation, small geometric details that did not substantially affect the global structural response were eliminated or simplified as needed. During the model preparation process, the support regions and major load-transfer paths were maintained.

Material Properties

Oak wood and aluminium alloy were taken into account in the baseline analysis. While oak was considered as a lower-density structural option, aluminium was chosen as the traditional CubeSat structural material. Density, Young's modulus, Poisson's ratio, and the tensile yield strength value used for factor-of-safety computations were among the finite element material inputs. Young's modulus and Poisson's ratio controlled the chassis's elastic deformation, while density dictated the inertial force produced by the applied 10 g body acceleration.

The aluminium model weighed 0.31978 kg for the same chassis geometry, while the wooden model weighed 0.10802 kg. Thus, the mass of the wooden chassis was about one-third that of the complete aluminium chassis. Although wood has direction-dependent mechanical characteristics and is sensitive to moisture content, the current study used an isotropic material model to represent oak in order to facilitate a straightforward direct comparison with aluminium (Güntekin et al., 2016; Chakkour and Perré, 2024; Tippner et al., 2022).

Table 1. Material properties used for the aluminium alloy and oak wood finite element models. Material properties were obtained from the ANSYS Engineering Data material definitions used in the finite

element models. Wood was represented using the isotropic oak properties adopted for the present comparative analysis.

Material Property	Aluminum Alloy	Wood (Oak)
Density (kg/m³)	2770	935.7
Young's Modulus (GPa)	71	22.78
Poisson's Ratio	0.33	0.3742
Tensile yield strength (MPa)	280	47.76

Mesh and Finite Element Model

Three-dimensional tetrahedral solid elements were used in ANSYS Mechanical to carry out the structural simulations. Because the CubeSat chassis had thin members, rail interfaces, openings, and intersecting geometric features that made a fully structured mesh impractical, tetrahedral elements were chosen.
To enhance mesh generation, small non-structural geometric features were simplified as needed. In order to reduce computational costs, coarser elements were kept in less critical areas while local refinement was applied close to joints, corners, rail interfaces, and other areas anticipated to contain higher stress gradients.

To prevent variations in finite element discretisation from introducing differences in structural response, the same meshing technique was applied to the wooden and full aluminium baseline models. Standard element-quality metrics, such as skewness and orthogonal quality, were used to evaluate mesh quality (Frey and George, 2008; Knupp, 2001; Shewchuk, 2002).

Launch Loading and Boundary Conditions

As a simplified launch-loading condition, each chassis was subjected to a quasi-static acceleration of 10 g, or 98.1 m/s². The matching inertial force was calculated using

$$F = ma$$

where a is the applied acceleration and m is the mass of the chassis. Under the same acceleration, the aluminium and wooden chassis produced different self-inertial loads due to their disparate densities and masses. As a result, the heavier aluminium chassis underwent more inertial loading than the wooden chassis.

At the chassis's base mounting locations, fixed supports were installed. To guarantee a consistent comparison, both baseline models had the same acceleration direction and support locations.

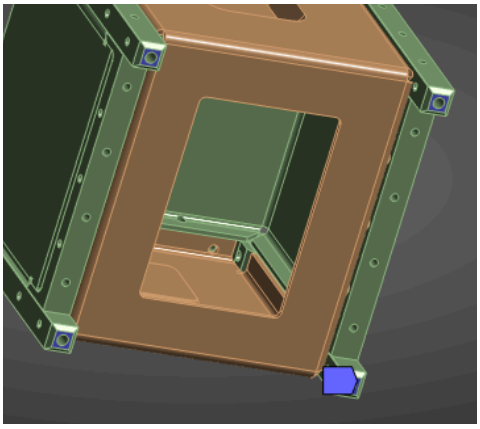


Figure 3. Fixed-support regions applied at the deployer interface of the CubeSat chassis for the 10 g quasi-static launch simulation.

Baseline Simulation and Mass Comparison

The same geometry, mesh strategy, support locations, acceleration direction, and solver settings were used to analyse the wooden and full aluminium chassis. The main distinction between the two baseline simulations was the assigned material.

The full aluminium chassis weighed 0.31978 kg under the same geometry, whereas the wooden chassis weighed 0.10802 kg. As a result, the aluminium chassis weighed 2.96 times more. This mass difference also increased the aluminium chassis's self-inertial loading since the loading was applied as body acceleration.

For the ensuing topology optimisation of the aluminium chassis, equivalent von Mises stress, total deformation, and factor of safety were taken from the baseline analyses.

Equivalent Stress Results

The full aluminium chassis developed a maximum equivalent von Mises stress of 0.73 MPa under the 10 g body acceleration, whereas the wooden chassis developed a lower maximum stress of 0.247 MPa. Both values came straight from the corresponding finite element analyses.

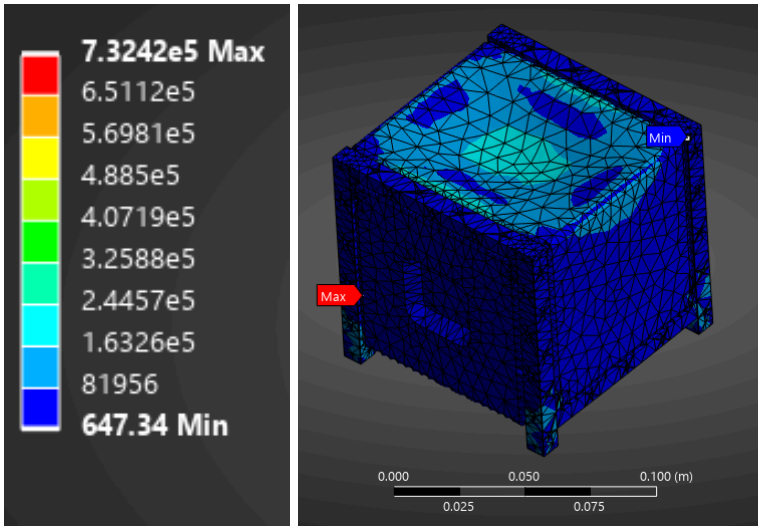


Figure 4. Equivalent von Mises stress distribution of the full aluminium CubeSat chassis under the 10 g quasi-static loading condition. Stress values in the ANSYS contour legend are displayed in Pa (maximum = 7.32×10^5 Pa, equivalent to approximately 0.73 MPa).

With the highest stresses occurring close to the rail-to-panel junctions and decreasing towards the less heavily loaded panel regions, both chassis maintained the same principal load-transfer geometry. However, under the same 10 g acceleration, the peak stress developed decreased due to the wood's lower density, which also decreased the amount of inertial loading.

Total Deformation Results

Due to their similar geometry and boundary constraints, the aluminium and wooden CubeSat chassis showed comparable deformation patterns. In both situations, the maximum deformation happened close to the upper panel's centre and diminished as it approached the fixed-support areas at the base.

The wooden chassis showed a slightly greater maximum deformation of 1.66 µm than the aluminium chassis, which had a maximum total deformation of 1.62 µm. The overall deformation under the modelled loading condition was very similar, as evidenced by the difference of about 2.5%.

Wood's significantly lower density results in a lower inertial load under the same body acceleration even though it has a lower elastic modulus than aluminium. Thus, the lower stiffness of the wooden chassis is partially offset by the decrease in applied inertial force, leading to comparable overall deformation under the simulated loading condition.

Factor of Safety Analysis

The factor of safety (FOS) was calculated as the ratio of the tensile yield strength to the maximum equivalent von Mises stress developed under the applied loading condition:

$$\mathrm{FOS} = \frac{\sigma_y}{\sigma_{\mathrm{vM,max}}}$$

For the full aluminum chassis,

$$FOS_{Al} = \frac{280\ MPa}{0.73\ MPa} = 383.6$$

For the wooden chassis,

$$FOS_{wood} = \frac{47.76\ MPa}{0.247\ MPa} = 193$$

Thus, under the simulated 10 g self-inertial loading condition, both chassis remained significantly below their respective tensile yield strengths. Although the wooden chassis only had roughly one-third of the aluminium mass, it still showed a high factor of safety. However, the full aluminium chassis maintained the larger calculated safety margin.

The comparison demonstrates that, despite having a lower tensile yield strength, the wooden chassis was able to maintain a significant factor of safety because the lower density of wood decreased the inertial stress created under the same body acceleration.

Summary of Baseline Static Structural Results

The baseline results demonstrate that, despite having only about one-third of the mass of the full aluminium chassis, the wooden chassis developed lower equivalent stress and almost the same deformation. Under the same 10 g self-inertial loading condition, the wooden chassis maintained a factor of safety of 193, whereas the full aluminium chassis maintained a higher factor of safety of 383.6.

These findings demonstrate that the inertial stress produced during acceleration was significantly decreased by the wood's lower density. As a result, despite having a lower tensile yield strength, the wooden chassis maintained a sizeable calculated safety margin, which served as the foundation for comparison with the topology-optimised aluminium design.

Table 2. Baseline structural comparison of the aluminium and wooden CubeSat chassis under 10 g body acceleration.

Parameter	Aluminum Chassis	Wooden Chassis
CAD geometry	Identical baseline geometry	Identical baseline geometry
Structural volume	Same	Same
Mesh	Same	Same
Boundary conditions	Same fixed-support regions	Same fixed-support regions
Applied body acceleration	10 g	10 g
Acceleration magnitude (m/s²)	98.1	98.1
Mass (kg)	0.31978	0.10802
Maximum equivalent von Mises stress (MPa)	0.73	0.247
Maximum total deformation (µm)	1.62	1.66
Tensile yield strength (MPa)	280	47.76
Factor of safety	383.6	193
Primary stress-concentration region	Rail-to-panel junctions	Rail-to-panel junctions
Maximum-deformation region	Centre of the upper panel	Centre of the upper panel
Minimum-deformation region	Fixed-support regions	Fixed-support regions

TOPOLOGY OPTIMIZATION AND OPTIMIZED STRUCTURAL ANALYSIS

Optimization Objective and Setup

The wooden chassis weighed 0.10802 kg, while the entire aluminium chassis weighed 0.31978 kg. Therefore, in order to match the wooden chassis, the aluminium mass would need to be decreased by

$$R_m = \left(1 - \frac{m_{\text{wood}}}{m_{\text{Al}}}\right) \times 100$$

$$R_m = \left(1 - \frac{0.10802\ \text{kg}}{0.31978\ \text{kg}}\right) \times 100\% = 66.2\%$$

Thus, a 66.2% decrease in aluminium mass was the theoretical equal-mass target. The solved aluminium baseline model was used for topology optimisation. The material characteristics, support conditions, and 10 g body acceleration were all kept constant. The primary structural load paths were maintained by protecting deployer interfaces, support areas, and crucial connection elements from material removal.

Topology Optimization Procedure

The solved full-aluminium chassis was used as the reference design for the topology optimisation in ANSYS Structural Optimisation (ANSYS, 2024a; ANSYS, 2024b). The initial optimisation target was based on the mass difference between the wooden and full-aluminium chassis. Since the wooden chassis

had a mass of 0.10802 kg compared with 0.31978 kg for the full-aluminium chassis, an aluminium mass reduction of 66.2% would theoretically have been required to obtain an aluminium structure of equivalent mass:

The 66.2% value was therefore used as the initial theoretical mass-reduction target. However, when this level of material removal was applied to the present chassis, the resulting topology did not retain a continuous load-carrying geometry. Material removal caused separation between structural regions, making the resulting configuration unsuitable for subsequent structural analysis as a continuous chassis. The mass-reduction constraint was therefore progressively relaxed until the optimisation produced a single continuous load-carrying geometry. The final continuous configuration had a mass of 0.211 kg, corresponding to a 34% reduction relative to the full-aluminium baseline:

$$R_m = \frac{0.31978\ \text{kg} - 0.211\ \text{kg}}{0.31978\ \text{kg}} \times 100\% = 34\%$$

The 34% reduction obtained here is specific to the topology-optimisation problem defined in this study and should not be interpreted as a general limit on aluminium mass reduction. The amount of material that can be removed while retaining structural continuity depends on the initial chassis geometry, the preserved regions, the locations through which structural members must remain connected, the applied boundary and loading conditions, and the optimisation constraints. Under the particular combination of geometry and constraints used in the present model, the theoretical 66.2% target caused loss of continuity, whereas the 34% reduction produced a continuous chassis suitable for reanalysis. A different chassis geometry, arrangement of preserved regions, loading condition, or optimisation setup could therefore permit a different degree of mass reduction. Consequently, 34% represents the continuous optimised configuration identified for the present model rather than an inherent maximum mass-reduction capability of aluminium CubeSat structures.

The resulting 0.211 kg optimised geometry was subsequently reanalysed using the same aluminium material properties, fixed-support conditions, and 10 g body acceleration used for the full-aluminium baseline. This allowed the structural response of the optimised chassis to be compared directly with the wooden and full-aluminium configurations under the same analysis conditions.

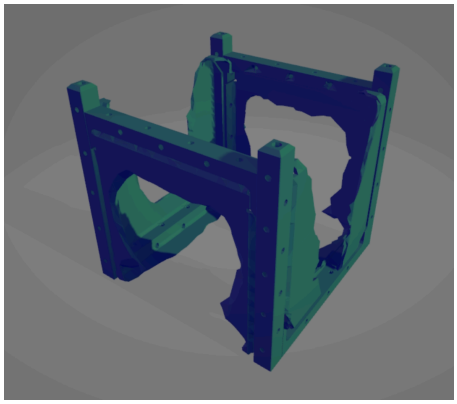


Figure 5. Topology-optimised aluminium CubeSat chassis after 34% mass reduction while maintaining a continuous load-carrying structure.

Optimized Aluminum Structural Results

The optimised aluminium chassis was assessed using the same fixed-support and 10 g body acceleration parameters as the baseline model. 1.27 MPa was the highest equivalent von Mises stress. The matching factor of safety, using the aluminium tensile yield strength value of 280 MPa, was

$$FOS_{Al,opt} = \frac{280\ MPa}{1.27\ MPa} = 220$$

As a result, even though its factor of safety dropped from 383.6 for the full aluminium chassis to 220, the optimised chassis maintained a high calculated safety margin following the 34% mass reduction.

Table 3. Final comparison of the wooden, full aluminium, and topology-optimised aluminium CubeSat chassis under 10 g body acceleration.

Parameter	Wooden Chassis	Full Aluminum Chassis	Optimized Aluminum Chassis
Mass (kg)	0.10802	0.31978	0.211
Mass reduction (%) from full aluminum	—	—	34%
Maximum equivalent von Mises stress (MPa)	0.247	0.73	1.27
Factor of safety	193	383.6	220

Final Comparison

Although it was still almost twice as heavy, the optimised aluminium chassis maintained a slightly higher factor of safety than the wooden chassis. The optimised aluminium design achieved a factor of safety of

220 at 0.211 kg, while wood achieved a factor of safety of 193 at a mass of 0.10802 kg. Therefore, under the modelled 10 g self-inertial loading condition, topology optimisation decreased the mass penalty of aluminium but did not eliminate the mass-efficiency advantage of wood.

DISCUSSION

The findings demonstrate that because inertial force is dependent on chassis mass, lower structural mass can significantly affect the factor of safety under acceleration-driven loading. Despite having a lower tensile yield strength than aluminium, the self-inertial stress created under the same 10 g acceleration was lessened by wood's significantly lower density.

Despite being almost twice as heavy, the topology-optimised aluminium chassis maintained a factor of safety of 220, which was only slightly higher than the wooden chassis value of 193. The optimised geometry lost structural continuity as a result of the theoretical 66.2% mass reduction needed to match the wooden chassis.

The wooden chassis offered a more mass-efficient combination of low structural mass and high factor of safety under the modelled conditions. This does not mean that wood is always better than aluminium, but it does demonstrate that absolute material strength is not enough for assessing CubeSat structures that are lightweight. Therefore, structural mass and the inertial loading caused by that mass should be considered when interpreting the factor of safety.

Limitations

One 10 g quasi-static loading condition and one CubeSat chassis geometry were taken into consideration in this study. As a result, vibration, shock, buckling, thermal, and deployment environments are not represented by the results. The simulations did not incorporate a common internal payload mass and only took chassis self-inertia into account. More spacecraft hardware could change the relative structural response of the materials and add more inertial loads.

Although real wood is anisotropic and sensitive to material variability, moisture content, and grain direction, oak was represented using an isotropic material model. This simplification does not account for the direction-dependent stiffness and strength associated with wood grain orientation. Therefore, the calculated stress and factor of safety should be interpreted as results of the simplified isotropic oak model rather than exact predictions for a physical wooden chassis.

Lastly, the optimisation constraints, preserved regions, and current chassis geometry all contributed to the 34% reduction in aluminium mass. It should not be interpreted as a general mass-reduction limit for aluminium CubeSat structures; rather, it represents the continuous optimised configuration found in this study.

CONCLUSION

This study used the same 10 g self-inertial loading condition to compare CubeSat chassis made of full aluminium, wood, and topology-optimised aluminium. Although the full aluminium chassis had the highest mass, it also achieved the highest factor of safety. Topology optimisation resulted in a final mass of 0.211 kg and a factor of safety of 220 by reducing the aluminium chassis mass by 34%. However, at a significantly lower mass of 0.10802 kg, the wooden chassis attained a factor of safety of 193.

As a result, the optimised aluminium chassis remained almost twice as heavy while maintaining only a slight factor-of-safety advantage. The wooden chassis offered a more mass-efficient combination of low structural mass and high factor of safety under the modelled conditions. These findings demonstrate that safety margin and structural mass, rather than just absolute material strength, should be used to evaluate CubeSat structural materials.

REFERENCES

1. National Aeronautics and Space Administration. (2026). What are SmallSats and CubeSats?
2. California Polytechnic State University. (2022). CubeSat Design Specification, Revision 14.1. California Polytechnic State University, San Luis Obispo.
3. Elshaal, A., Okasha, M., Sulaeman, E., Jallad, A. H., Aizat, W. F., & Alzubaidi, A. B. (2024). Structural analysis of AlAinSat-1 CubeSat. The Egyptian Journal of Remote Sensing and Space Sciences, 27(3), 532–546. https://doi.org/10.1016/j.ejrs.2024.06.006
4. Alhammadi, A., Jarrar, F., Al-Shaibah, M., Almesmari, A., Vu, T. Q., Tsoupos, A., & Marpu, P. R. (2020). Effect of finite element model details in structural analysis of CubeSats. CEAS Space Journal. https://doi.org/10.1007/s12567-020-00339-z
5. Alhammadi, A., Jarrar, F., & Marpu, P. (2019). Quasi-static and dynamic response of a 1U nanosatellite during launching. Proceedings of the 8th European Conference for Aeronautics and Space Sciences.
6. Park, Y.-K., Kim, G.-N., & Park, S.-Y. (2021). Novel structure and thermal design and analysis for CubeSats in formation flying. Aerospace, 8(6), 150. https://doi.org/10.3390/aerospace8060150
7. Capovilla, G., Cestino, E., Reyneri, L. M., & Romeo, G. (2020). Modular multifunctional composite structure for CubeSat applications: Preliminary design and structural analysis. Aerospace, 7(2), 17. https://doi.org/10.3390/aerospace7020017
8. Murphy, D. M., Abou-Ghanem, M., Cziczo, D. J., Froyd, K. D., Jacquot, J., Lawler, M. J., Maloney, C., Plane, J. M. C., Ross, M. N., Schill, G. P., & Shen, X. (2023). Metals from spacecraft reentry in stratospheric aerosol particles. Proceedings of the National Academy of Sciences, 120(43), e2313374120. https://doi.org/10.1073/pnas.2313374120
9. Ferreira, J. P., Huang, Z., Nomura, K., & Wang, J. (2024). Potential ozone depletion from satellite demise during atmospheric reentry in the era of megaconstellations. Geophysical Research Letters, 51, e2024GL109280. https://doi.org/10.1029/2024GL109280

10. Murata, K., Nakamura, M., Kariya, K., Tsuchiya, M., Yamashiki, Y. A., & Doi, T. (2024). Space exposure test of hardwood specimens in the International Space Station. Journal of Wood Science, 70, 49. https://doi.org/10.1186/s10086-024-02165-x
11. Ross, R. J. (Ed.). (2010). Wood handbook: Wood as an engineering material. General Technical Report FPL-GTR-190. U.S. Department of Agriculture, Forest Service, Forest Products Laboratory.
12. Forest Products Laboratory. (2021). Wood handbook: Wood as an engineering material. General Technical Report FPL-GTR-282. U.S. Department of Agriculture, Forest Service, Forest Products Laboratory. https://doi.org/10.2737/FPL-GTR-282
13. Frey, P. J., & George, P.-L. (2008). Mesh generation: Application to finite elements (2nd ed.). Wiley.
14. Knupp, P. M. (2001). Algebraic mesh quality metrics. SIAM Journal on Scientific Computing, 23(1), 193–218. https://doi.org/10.1137/S1064827500371499
15. Shewchuk, J. R. (2002). What is a good linear finite element? Interpolation, conditioning, anisotropy, and quality measures. University of California, Berkeley.
16. Zhu, J. H., Zhang, W. H., & Xia, L. (2016). Topology optimisation in aircraft and aerospace structure design. Archives of Computational Methods in Engineering, 23(4), 595–622. https://doi.org/10.1007/s11831-015-9151-2
17. Peng, L., Shen, X., Dong, S., & Fang, Y. (2025). Topology optimisation methods and their applications in aerospace: A review. Structural and Multidisciplinary Optimization. https://doi.org/10.1007/s00158-025-04030-x
18. ANSYS. (2024a). Topology optimization: Density-based solution methodology. ANSYS Mechanical Structural Optimization Documentation.
19. ANSYS. (2024b). Response constraints in topology optimization. ANSYS Mechanical Structural Optimization Documentation.
20. Tortora, P. (2020). Small satellites beyond boundaries. CEAS Space Journal, 12, 489–490. https://doi.org/10.1007/s12567-020-00336-2
21. Güntekin, E., Yılmaz Aydın, T., & Niemz, P. (2016). Some orthotropic mechanical properties of sessile oak (Quercus petraea) as influenced by moisture content. Eurasian Journal of Forest Science, 4(1), 40–47. https://doi.org/10.31195/ejejfs.258624
22. Chakkour, T., & Perré, P. (2024). Developing the orthotropic linear-elastic model for wood applications using the FE method. Materials Advances, 5, 7747–7765. https://doi.org/10.1039/D4MA00554F
23. Tippner, J., Milch, J., Sebera, V., & Brabec, M. (2022). Elasto-plastic material model of oak at two moisture content levels. Holzforschung, 76(10), 886–896. https://doi.org/10.1515/hf-2022-0008
24. Lima, V. H. L. C., Rodrigues, R. N., Lamary, P. M. C., & Bezerra, R. A. (2022). Dynamic structural analysis in a 2U CubeSat considering quasi-static loads. Ingeniare: Revista Chilena de Ingeniería, 30(1), 94–108. https://doi.org/10.4067/S0718-33052022000100094
25. Gao, B., Yang, H., Chen, W., & Wang, H. (2024). Topology optimization of the bracket structure in the acquisition, pointing, and tracking system considering displacement and key point stress constraints. Aerospace, 11(11), 939. https://doi.org/10.3390/aerospace11110939